15. COUPLED EARLY PLIOCENE–MIDDLE MIOCENE BIO-CYCLOSTRATIGRAPHY OF SITE 1006 REVEALS ORBITALLY INDUCED CYCLICITY PATTERNS OF GREAT BAHAMA BANK CARBONATE PRODUCTION[1]

D. Kroon,[2] T. Williams,[3] C. Pirmez,[4] S. Spezzaferri,[5] T. Sato,[6] and J.D. Wright[7]

ABSTRACT

Detailed biostratigraphy in Site 1006 based on planktonic foraminifers and nannofossils shows large-scale sedimentation rate variability in the Florida Strait west of the Great Bahama Bank. A 'floating' cyclostratigraphy based mainly on resistivity logs and magnetic susceptibility data has been fixed to the biostratigraphy in the absence of magnetostratigraphy. The strongest orbital cycle present is the precessional beat, which is present in the borehole logs throughout the record. Counting the cycles resulted in an accurate time scale and thus a sedimentation rate time series.

Spectral analysis of the sedimentation rate time series shows that the short-term cycle of eccentricity (~125 k.y.) and the long term cycle of eccentricity (~400 k.y.) are pervasive throughout the Miocene record, together with the long-term ~2-m.y. eccentricity cycle. The Great Bahama Bank produced pulses of shallow carbonate input once every precessional (sea level) cycle during the Miocene and perhaps two pulses per cycle in the early Pliocene. The amount of sediment exported in these pulses appears to be controlled by eccentricity modulation of the precessional amplitude and therefore the amplitude of the sea-level rise. Finally, an increase in sedimentation rate just after the Miocene/Pliocene boundary is attributed to a change in the location and strength of sediment drift currents in the Florida Strait due to reorganization of the currents following the closure of the Panama Isthmus.

INTRODUCTION

Site 1006 is located in 658 m of water in the northern portion of the Santaren Channel ~30 km from the western platform edge of the Great Bahama Bank (Fig. 1). It is the most distal member of five transect sites drilled during Leg 166. Site 1006 was positioned on a thick, continuous sequence of Neogene-aged drift sediments. The sediment drifts interfinger with prograding carbonate bank deposits in the Florida Strait.

We attempted to date the sedimentary section as accurately as possible by using a combination of detailed biostratigraphy and cyclostratigraphy to document sedimentation rate changes at Site 1006. Cyclostratigraphy allows the use of the characteristics of variations in the Earth's orbital elements for producing a measure of time that results in a detailed chronostratigraphy. Recent studies have shown that orbitally induced time series can be obtained from Pliocene and Miocene sections (Hilgen, 1991; Hilgen et al., 1995; Shackleton et al., 1990). Here, we use the cyclostratigraphic technique to date the cyclic sequence of Site 1006. The Leg 166 shipboard party described the presence of pervasive cyclicity in the entire middle Miocene–lower Pliocene section (Eberli, Swart, Malone, et al., 1997). The cyclicity is attributed to sea-level changes that result in fluctuations in

sediment production by the carbonate factory of the Great Bahama Bank (Eberli, Swart, Malone, et al., 1997). Delivery of neritic carbonate material to the basin during sea-level highstands results in expanded sections compared to erosion or starved sedimentation of pelagic and siliciclastic material during sea-level lowstands (Droxler and Schlager, 1985; Reijmer et al., 1988). This alternating pattern of deposition has dominated sedimentation near platforms and has also occurred at Site 1006 in the Pleistocene (Kroon et al., Chap. 2, this volume; Rendle et al., Chap. 6, this volume). There is no reason to assume that this pattern did not prevail in the Miocene–Pliocene period; thus, we assume that detailed sedimentation rate changes reflect fluctuations in carbonate platform productivity in relation to sea-level changes.

Whole-core measurement of magnetic susceptibility and downhole resistivity logs (SFLU and FMS) were used to sample the cyclic section. Unfortunately, only a single hole was drilled in the Miocene–lower Pliocene part of the section, but logging of the hole ensured a complete documentation of the cycles. The section is highly expanded, so that all the cycles can be resolved on the resistivity logs, and particularly in the FMS images. To calculate time, we mostly used the downhole logs rather than the whole-core magnetic susceptibility variations because of the possibility of core gaps. The sedimentation rates based on detailed biostratigraphy demonstrate that the dominant cycle present in the logs is compatible with the Earth's precessional cycle. In the unfortunate absence of magnetostratigraphy, time was calculated from the cycle record for the upper Miocene–lower Pliocene section of Site 1006, and this period of time was then anchored to a biostratigraphic event with a well-known absolute age.

In this paper, we show that the variability of platform production relates to precessionally induced sea-level changes. Moreover, we show that the thickness rather than the amplitude of the precessional sediment cycles is modulated at longer periods, which are very similar to known cycles of orbital eccentricity, at periods of ~125 k.y. ~400 k.y., and ~2000 k.y. Hence, we infer that eccentricity plays an important role in modulating the amplitude of sea-level change in the middle-late Miocene period.

[2]Department of Geology and Geophysics, University of Edinburgh, Grant Institute, West Mains Road, Edinburgh EH9 3JW, Scotland, United Kingdom. D.Kroon@glg.ed.ac.uk

[3]Leicester University Borehole Research, Department of Geology, Leicester University, Leicester, LE1 7RH, United Kingdom.

[4]Borehole Research Group, Lamont-Doherty Earth Observatory, Columbia University, Palisades NY 10964-8000, USA. (Present address: Deepwater Reservoirs Group, Exxon Production Research Co., PO Box 2189, Houston TX 77252, USA.)

[5]Geological Institute, ETH-Zentrum, 8092 Zürich, Switzerland.

[6]Institute of Applied Earth Sciences, Mining College, Akita University, Tegata Gakuencho 1-1, Akita 010, Japan.

[7]Department of Geological Sciences, Rutgers University, Piscataway NJ 08854-8066, USA.
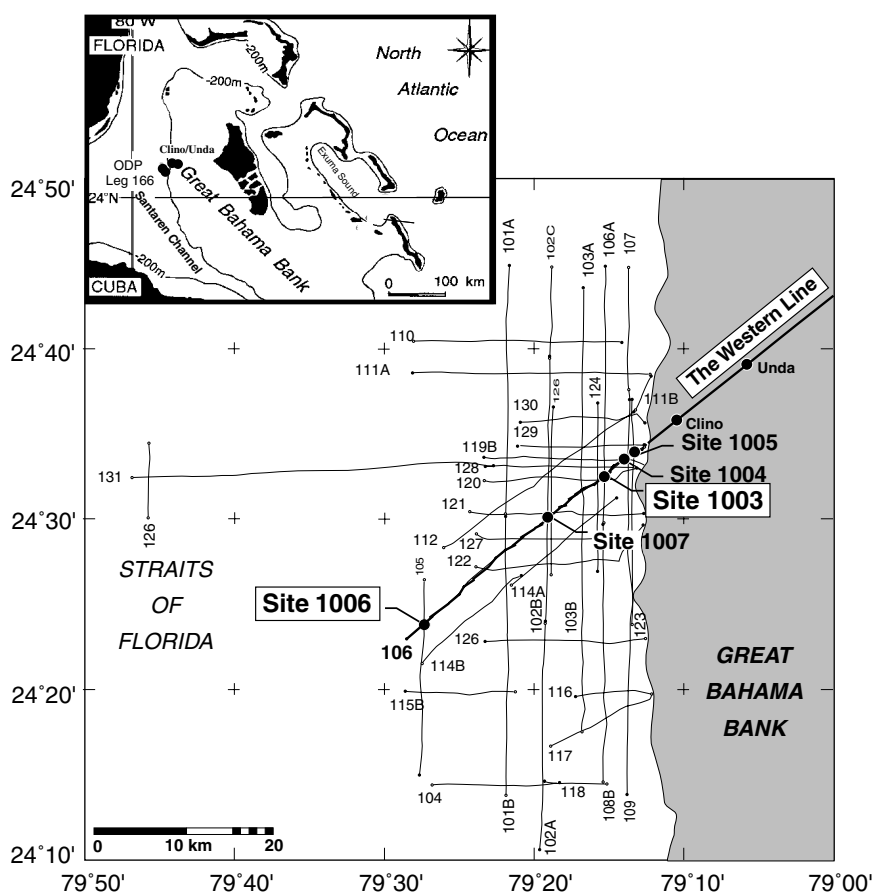
Figure 1. Location map of Site 1006 in the Florida Strait among the other sites drilled during Leg 166. Site 1006 is the most distal site along the transect perpendicular to the Great Bahama Bank carbonate platform.

RESULTS: MIDDLE MIOCENE TO EARLY PLIOCENE BIOSTRATIGRAPHY AND CYCLOSTRATIGRAPHY

The shipboard early Pliocene to middle Miocene biostratigraphy of Site 1006 has been refined for this paper, and the main results are described here. These results include (1) the planktonic foraminiferal biostratigraphy, (2) nannofossil biostratigraphy, and (3) cyclostratigraphy. Unfortunately, we could not use the cyclostratigraphy for re-dating the biohorizons because of the level of uncertainty in the picked beds, the absence of eccentricity control on the amplitude of the resistivity-log cycle peaks, and the lack of magnetostratigraphy. Thus only a 'floating' cyclostratigraphy was produced. The 'floating' stratigraphy represents a period of time that needs to be attached to a certain biostratigraphic datum level with a well-known absolute age to obtain a time frame for the entire 'floating' section.

Planktonic Foraminiferal Events

Planktonic and benthic foraminifers of the middle Miocene–early Pliocene assemblages are very well preserved and abundant throughout this interval. Reworking and contamination of older specimens and/or shallow-water benthic species are very rare or absent. Reworking generally consists of rare specimens of shallow-water benthic foraminifers and of older planktonic foraminifer species such as Eocene turborotaliids or Oligocene *Paragloborotalia pseudokugleri.*

Planktonic foraminiferal faunas from Hole 1006A are very rich in tropical warm-water species; therefore, the low-latitude standard zonation of Blow (1969, 1979), with slight modification by Kennett and Srinivasan (1983) and Curry, Shackleton, Richter, et al. (1995), was applied for the biostratigraphy of Site 1006, following the criteria used in Eberli, Swart, Malone, et al. (1997; see also Wright and

Kroon, Chap. 1, this volume). The datum levels at Site 1006 are presented in Figure 2. Assigned ages for the datum levels that we used in the first instance to calculate sedimentation rates are from Berggren et al. (1995a, 1995b), except for the first occurrence of *Globigerinoides conglobatus* at 6.2 Ma (Chaisson and Pearson, 1997). The major bioevents used in this study for the identification of the zonal boundaries and zones are presented in Figure 2, and the planktonic foraminiferal datum levels are summarized in Table 1 (back-pocket foldout, this volume) and Table 2. The following zones have been recognized.

Zone N12

Interval: Sample 166-1006A-77X-2, 90–92 cm, to 72X-2, 72–74 cm, ~48.4 m thick
Definition: Interval from the first occurrence (FO) of *Fohsella fohsi* to the last occurrence (LO) of the *Fohsella* group

The base of this zone was not observed in the studied samples because *F. fohsi* together with *Fohsella praefohsi* and *Fohsella peripheroacuta* are present from the base of the sequence. *Fohsella fohsi lobata* first occurs in Sample 166-1006A-73X-3, 137–140 cm, at 673.57 mbsf. This bioevent is equated to be 12.5 Ma (Berggren et al., 1995a, 1995b) The last samples attributed to this zone contain the FO of *Fohsella fohsi robusta* which is equated to be 12.10 Ma; therefore, the top of the zone (which is equated to be 11.9 Ma) may be condensed at Hole 1006A, or nonrecovery (Fig. 2) may account for the absence of the upper boundary of this zone.

Planktonic foraminiferal assemblages of Zone N12 are also characterized by common *Orbulina universa, Dentoglobigerina baroemoenensis, Dentoglobigerina altispira, Globigerinoides ruber, Globigerinoides sacculifer, Globorotalia scitula, Globorotalia archeomenardii, Globoquadrina dehiscens, Zeaglobigerina woodi, Para-*
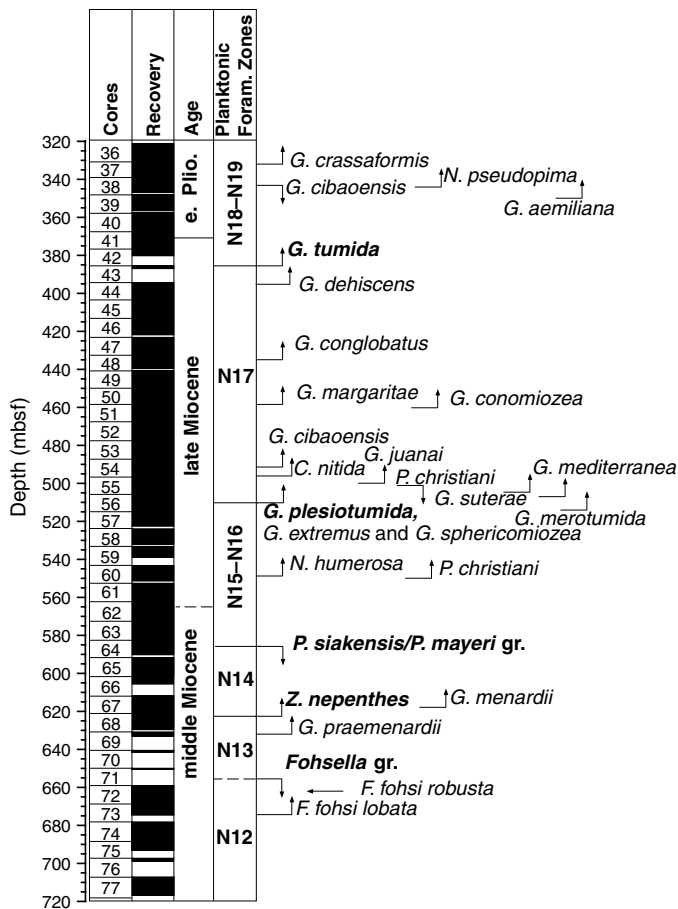
Figure 2. Planktonic foraminiferal biostratigraphy at Site 1006 (Hole 1006A) for the lower Pliocene–middle Miocene interval. Zonal indicators are in bold.

Table 2. Position of main planktonic foraminiferal biostratigraphic events.

Bioevent	Core, section, interval (cm)	Depth (mbsf)	Age (Ma)
	166-1006A-		
FO G. crassaformis	37X-1, 85–90	331.45	4.50
LO G. cibaoensis	38X-3, 85–90	343.65	**4.60**
FO G. aemiliana	40X-1, 85–90	358.95	—
FO N. pseudopima	40X-5, 85–90	364.95	—
FO G. tumida	43X-1, 85–90	385.95	5.60
LO G. dehiscens	44X-1, 85–90	395.05	5.80
LO G. laenguaensis	44X-1, 85–90	395.05	**6.00**
FO G. conglobatus	48X-2, 135–137	434.85	6.20
FO G. margaritae	50X-6, 85–90	458.45	6.40
FO G. conomiozea	51X-1, 85–90	460.15	7.12
FO G. cibaoensis	54X-3, 85–90	491.05	**7.80**
FO C. nitida	54X-6, 85–90	495.55	8.10
FO G. juanai	55X-3, 85–90	500.15	8.10
LO P. christiani	55X-4, 85–90	501.65	—
FO G. suterae	55X-6, 85–90	504.65	**7.80**
FO G. mediterranea	56X-1, 85–90	506.25	—
FO G. plesiotumida	56X-3, 85–90	509.25	8.30
FO G. extremus	56X-3, 85–90	509.25	8.30
FO G. sphericomiozea	56X-3, 85–90	514.25	—
FO G. merotumida	57X-2, 85–90	517.35	—
FO N. humerosa	60X-3, 85–90	547.75	8.50
FO P. christiani	60X-4, 85–90	549.25	—
LO P. siakensis/P. mayeri gr.	64X-3, 85–90	586.25	11.40
FO N. acostaensis	65X-5, 85–90	598.95	—
FO G. menardii	67X-5, 85–90	618.25	—
FO Z. nepenthes	68X-1, 85–90	621.85	11.80
FO G. praemenardii	69X-1, 85–90	631.35	—
FO F. fohsi robusta	72X-2, 72–74	661.72	12.10
FO F. fohsi lobata	73X-3, 137–140	673.57	12.50
FO G. archaeomenardii	75X-3, 35–37	691.70	—

Notes: FO = first occurrence, LO = last occurrence. Less reliable events are given in bold; — = unreliable events.

gren et al., 1995b). However, they are considered here also as single species based on their peculiar differences (Spezzaferri, 1994), and informally grouped under the *P. siakensis/P. mayeri* group. Berggren et al. (1995b) equate the LO of *P. mayeri* to be 11.4 Ma.

Zones N15–N16

Interval: Sample 166-1006A-64X-2, 85–90 cm, to 56X-4, 85–90 cm; ~74 m thick

Definition: Interval from the LO of the *P. siakensis/P. mayeri* group to the FO of *Globorotalia plesiotumida.*

At Hole 1006A, Zones N15 and N16 are considered as a single interval. The lower boundary of Zone N15 is commonly identified with the LO of *P. mayeri* and the upper boundary with the FO of *Neogloboquadrina acostaensis*. This latter species was also traditionally used to separate the upper and middle Miocene (N15/N16 boundary) (Blow, 1979; Berggren et al., 1995b). At Hole 1006A, the two species occur together in Sample 166-1006A-65X-5, 85–90 cm, belonging to Zone N14; therefore, Zone N15 as traditionally described was not observed at Hole 1006A. The co-occurrence of *P. mayeri* and *N. acostaensis* was observed by Spezzaferri (1998) in the North Atlantic, Spezzaferri et al. (unpubl. data) in South Italy, and Foresi et al. (1998) in the Mediterranean basin. Moreover, the FO of *N. acostaensis* is reported from middle Miocene sediments by Spiegler and Müller (1992), Müller and Spiegler (1993), and Rio (pers. comm., 1992). Therefore, it is reasonable to assume that the sedimentary sequence at Hole 1006A is continuous and the hiatus, which spans Zone N15 and was identified by shipboard analysis (Eberli, Swart, Malone, et al., 1997), is not present.

Three additional bioevents are identified in this interval. In Sample 166-1006A-60X-4, 85–90 cm, the FO of *Polipheribola christiani* is observed. This poorly known species seems to be related to *Candeina nitida* and is regarded as its ancestor (Bolli and Saunders, 1985). It is reported from Zone N16 by Bolli and Saunders (1985). *Neogloboquadrina humerosa* occurs in Sample 166-1006A-60X-3, 85–90 cm, and is equated to 8.5 Ma. Finally, *Globorotalia merotumida* first occurs in Sample 166-1006A-57X-2, 85–90 cm.

globorotalia siakensis/Paragloborotalia mayeri group, and *Sphaeroidinellopsis* group. Rarer components are *Dentoglobigerina larmeui, Globorotalia lenguaensis, Globigerina falconensis, Globigerina bulbosa, Globigerina bulloides,* and *Globigerinoides obliquus.*

Zone N13

Interval: Sample 166-1006A-69X-1, 75–76 cm, to 68X-2, 85–90 cm; ~9.5 m thick

Definition: Interval from the LO of the *Fohsella* group to the FO of *Zeaglobigerina nepenthes*

Within this zone, *Globorotalia praemenardii* evolves from its ancestor *G. archeomenardii.*

Except for the absence of the *Fohsella* group, planktonic foraminiferal assemblages of this zone are similar to those observed for Zone N12.

Zone N14

Interval: Sample 166-1006A-68X-1, 85–90 cm, to 64X-3, 85–90 cm; ~35.5 m thick

Definition: Interval from the FO of *Z. nepenthes* to the LO of *P. mayeri*

In this zone, *Globorotalia menardii* evolves from its ancestor *G. praemenardii*. The top of Zone N14 is identified based on the LO of the *P. siakensis/P. mayeri* group instead of *P. mayeri* only. These two species belong to the same lineage and sometimes are considered as morphotypes of the same species (Bolli and Saunders, 1985; Berg-

157

The accompanying assemblage includes, among others, *O. universa, Sphaeroidinellopsis* group, *D. baroemoenensis, D. larmeui, G. scitula, G. lenguaensis, G. menardii, Globigerinella obesa, Globigerinella siphonifera, G. sacculifer, Globorotaloides hexagonus* and rarer *Streptochilus* spp.

Zone N17

Interval: Sample 166-1006A-56X-3, 85–90 cm, to 44X-1, 35–37 cm; ~113 m thick

Definition: Interval from the FO of *G. plesiotumida* to the FO of *Globorotalia tumida.*

Several additional bioevents are identified from this interval. The FO of *Globigerinoides extremus* coincides with the FO of *G. plesiotumida,* which is equated to be 8.3 Ma according to Berggren et al. (1995b) and Eberli, Swart, Malone, et al. (1997). At the same level, the first occurrence of *Globorotalia sphericomiozea* can be found. The FO of this species is reported by Berggren et al. (1995b) as young as 5.6 Ma and, therefore, much younger than in Hole 1006A. However, Barbieri (1998) identified this species in older sediments from the Atlantic coast northwest of Morocco.

The FO of *Globorotalia mediterranea* is observed in Sample 166-1006A-56X-1, 85–90 cm, and is very rare. The first occurrence of *Globorotalia suterae* is equated to be 7.8 Ma as calibrated in the Mediterranean area. In Hole 1006A this species is first observed in Sample 166-1006A-55X-6, 85–90 cm, below the FO of *C. nitida* (8.1 Ma). However, this discrepancy may be only apparent. Poore (1979) and Spezzaferri (1998) identified this species from early middle Miocene sediments in the North Atlantic and, therefore, the calibrated age may be the age of the migration of this species in the Mediterranean rather than its real first occurrence as observed in Hole 1006A.

The LO of *P. christiani* is observed in Sample 166-1006A-55X-4. 85–90 cm. Bolli and Saunders (1985) describe this species from Zone N16 only; however, since no evidence of displacement is found in Hole 1006A, its range should be extended to the base of Zone N17. The FO of *Globorotalia juanai* is observed in Sample 166-1006A-55X-3, 85–90 and is equated to be 8.1 Ma. This datum level is not applied here, because of the scarcity of this species in Hole 1006A. The FO of *C. nitida* in Sample 166-1006A-54X-6, 85–90 cm, is considered a more reliable bioevent for Hole 1006A because of the more continuous and abundant presence of this species throughout the sequence. *Globorotalia cibaoensis* first occurs in Sample 166-1006A-54X-3, 85–90 cm. Its FO is equated to be 7.8 Ma. The taxonomic interpretation of *G. cibaoensis* is very different from author to author and often it does not correspond to the original description of Bermudez (1949). Therefore, its datum levels are not used for the evaluation of the sedimentation rate, and their stratigraphic positions are only tentatively indicated in Figure 2.

The FO of *Globorotalia conomiozea* is observed in Sample 166-1006A-51X-1, 85–90 cm, and is equated to be 7.12 Ma. In Hole 1006A, this species is very rare and discontinuous and its FO may not be real; therefore, it is only tentatively indicated in Figure 2.

Globigerinoides conglobatus first occurs in Sample 166-1006A-48X-2, 135–137 cm, and is equated to be 6.2 Ma, whereas *Globorotalia margaritae* first occurs in 166-1006A-50X-6, 85–90 cm, and is equated to be 6.4 Ma. The LOs of both *G. lenguaensis* and *G. dehiscens* are in Sample 166-1006A-44X-1, 35–37 cm. These two bioevents are equated to be 6 and 5.8 Ma, respectively. The co-occurrence of the two species at the same level in Hole 1006A is probably due to the low recovery of Core 166-1006A-43X. The position of the two datums may lie within the missing 9.5 m of sediment between Sample 166-1006A-44X-1, 35–37 cm, and Sample 166-1006A-43X-1, 35–37 cm, according to the time scale of Berggren et al. (1995b).

With the exception of FO and LO of the above-mentioned species, the accompanying assemblages are similar to those described for the other zones and are typical of Atlantic low latitudes. The relatively abundant and continuous presence of *Streptochilus* spp. is remarkable.

Zones N18–N19

Interval: Sample 166-1006A-43X-1, 35.37 cm, to 36X-1, 81–86 cm, ~63.6 m thick

Definition: Interval from the FO of *Globorotalia tumida* to the FO of *Globorotalia miocenica*

At Hole 1006A, Zones N18 and N19 are considered as a single interval. The base of Zone N18 is placed with the FO of *G. tumida* and its top is not observed at Hole 1006A. The boundary between Zone N18 and N19 is based on the FO of *Sphaeroidinella dehiscens,* which has not been identified in the examined samples from Hole 1006A.

In this interval, the FO of *Globorotalia aemiliana* and the LO of *G. cibaoensis* are identified in Sample 166-1006A-40X-1, 85–90 cm, and 37X-2, 85–90 cm, respectively. The latter bioevent is equated to be 4.6 Ma. *Globorotalia aemiliana* evolves within this zone into *Globorotalia crassaformis* following the lineage proposed by Colalongo and Sartoni (1967); *Globorotalia hirsuta* (= *G. margaritae*)– *G. aemiliana*–*G. crassaformis.* Finally, also *Neogloboquadrina pseudopima* was first observed in Sample 166-1006A-40X-5, 85–90 cm. This species is not used here for the identification of Zone N20 because this species is also reported from the upper Zone N18 (Brönniman & Resig, 1971; Fleisher, 1974).

Planktonic foraminifer assemblages in this zone are very rich and diversified and include, among others, *O. universa, Sphaeroidinellopsis* group, *D. baroemoenensis, D. altispira, G. scitula, G. menardii, G. margaritae, G. suterae, G. dehiscens, Z. woodi, Z. nepenthes, G. falconensis, Gg. bulloides, G. obliquus, G. ruber, G. sacculifer, Globigerinoides trilobus, G. conglobatus, N. acostaensis* sinistral and dextral, *N. humerosa, Neogloboquadrina dutertrei,* and *G. siphonifera.* Minor components are *D. larmeui, G. obesa, G. bulbosa, Neogloboquadrina pachyderma* and *Streptochilus* spp.

The Miocene/Pliocene Transition

The Miocene/Pliocene boundary is currently defined by the age of the base of the Trubi Formation at Capo Rossello in Sicily (Cita and Gartner, 1973; Cita, 1975). Traditionally, the beginning of the Pliocene (the base of the Zanclean stage) is equated with evidence in the sedimentary record of the recovery of the Mediterranean Sea to full marine conditions after the "Messinian Salinity Crisis," when the basin became completely isolated (Ryan, Hsü, et al., 1973; Hsü, Montadert, et al., 1978; McKenzie at al., 1990; Spezzaferri et al., 1998). Sedimentary expression of this major event is a sharp lithologic change from an evaporative sequence topped with the "Lago Mare Facies" to pelagic sediments rich in planktonic foraminiferal faunas.

A sharp lithologic change at the Miocene/Pliocene boundary is not known to be present in geological records from the open ocean. In addition, this boundary does not correspond to any major biological event. Rather, it is characterized by a relatively low degree of biotic turnover (extinction plus origination) within all the microfossil groups and especially in planktonic foraminifers.

Blow (1969, 1979) placed the Miocene/Pliocene boundary within Zone N18, between the FOs of *G. tumida* and *S. dehiscens.* The FO of *G. tumida* is the bioevent most commonly accepted to identify this boundary in open ocean sequences (Premoli Silva et al., 1993; Berggren, 1973; Fleisher, 1974; Vincent, 1975; Berggren et al., 1995a, 1995b). However, based on the absence of marker species, the correlation between bioevents from the Mediterranean Sea and those from the open ocean remains difficult.

Since the Miocene/Pliocene boundary in the sequences from the Mediterranean Sea and the open ocean cannot be directly correlated using only bioevents, McKenzie et al. (in press) proposed to make an indirect correlation using the biostratigraphically derived sedimenta-

tion rates from the Bahamian sequence recovered at Hole 1006A to locate the age of the Miocene/Pliocene boundary as determined using the astronomically calibrated time scale as applied in the Mediterranean (Hilgen, 1991). Based on this correlation, we place the Miocene/Pliocene boundary at ~370–375 mbsf (tuned age of 5.33 Ma according to Hilgen, 1991) and the Zones MPL1/MPL2 boundary at ~361 mbsf (5.1 Ma according to Hilgen, 1991).

Nannofossil Events

Postcruise analysis of the calcareous nannofossil events was conducted to obtain a higher biostratigraphic resolution in the lower Pliocene–middle Miocene interval in Hole 1006A. The sampling distance for the lower Pliocene–middle Miocene interval is ~1.5–2 m for the nannofossil bioevents. The ages for the nannofossil events are derived from Berggren et al. (1995b). The zonal scheme established by Martini (1971) was used for the taxonomic interpretation. The datum levels are presented in Table 3.

The lower Pliocene is divided into three zones: Zones NN15, NN14–NN13, and NN12. The interval between the last appearances of *Sphenolithus abies* and *Amaurolithus* spp. defines NN15 (3.66–4.5 Ma). At Site 1006, the lower boundary of this interval occurs between Samples 166-1006A-28H-3, 114–115 cm, and 28H-5, 14–15 cm. Zones NN14 and NN13 are combined and are bounded by the LO of *Amaurolithus* spp. above and the first appearance of *Ceratolithus rugosus* between Samples 166-1006A-36X-1, 114–115 cm, and 36X-2, 14–15 cm.

At Site 1006, well-preserved specimens of *Discoaster quinqueramus* and *Discoaster berggrenii* can be found, marker species for upper Miocene Zone NN11. The total concurrent range of both species (5.6–8.6 Ma) defines Zone NN11. The highest occurrence of specimens of *D. quinqueramus* is present in Sample 166-1006A-38X-4, 64–65 cm. However, this occurrence is too high with respect to planktonic foraminiferal datum events; thus, the specimens in this sample are considered to have been reworked. Also, this occurrence is incompatible with the sedimentation rate changes based on the cyclostratigraphy (see "Early Pliocene–middle Miocene cyclostratigraphy" section). The basal occurrence of *D. berggrenii* is in Sample 166-1006A-54X, CC. In addition, useful datum levels such as *Amaurolithus amplificus* and *Amaurolithus primus* were found (Table 4). Zone NN10 ranges from the base of *D. quinqueramus* (8.6 Ma) to the last appearance of *Discoaster hamatus*. The base of Zone NN10 is placed between Samples 166-1006A-59X-3, 14–15 cm, and 59X-CC (538.05 mbsf). The total range of *D. hamatus* defines Zone NN9. The base of Zone NN9 was placed between Samples 166-1006A-52X-6, 14–15 cm, and 62X, CC.

Middle Miocene Zones NN6 through NN8 are recognized at Site 1006. The first appearance of *Catinaster coalitus* occurs at the NN7/NN8 boundary. This level is identified between Samples 166-1006A-66X-2, 14–15 cm, and 66X-CC. The base of Zone NN7 (13.2 Ma) is marked by the last appearance of *Cyclicargolithus floridanus*. This level is placed between Samples 166-1006A-75X-CC and 76X-1, 12–13 cm.

SEDIMENTATION RATES BASED ON PLANKTONIC FORAMINIFERAL BIOSTRATIGRAPHIC EVENTS

Sedimentation rate varies considerably based on biostratigraphy at Hole 1006A. It was calculated using 12 planktonic foraminiferal bioevents (Table 2) and the data are plotted on an age vs. depth curve as in Figure 3. We have used the planktonic foraminiferal events because some nannofossil events document reworking of very fine grained material in the section. The reworked specimens of some nannofossil species result in the presence of datum levels that are too highly positioned in the section shown in an age-depth plot in Figure 3, if sedimentation rates based on the planktonic foraminiferal biostratigraphy and cyclostratigraphy (see "Early Pliocene–middle Miocene cyclostratigraphy" section) are basically correct.

Calculated sedimentation rate varies from 1.32 to 19.25 cm/k.y. through the sequence. From the FO of *G. crassaformis* (4.5 Ma) to the FO of *G. tumida* (5.6 Ma), the sedimentation rate was ~4.9 cm/k.y. and from the FO of *G. tumida* to the LO of *G. dehiscens* (5.8 Ma) ~4.5 cm/k.y. However, because of the low recovery of Core 166-1006A-43X, the real LO of *G. dehiscens* may occur in the 9.5 missing meters. A significant shift in the sedimentation rate to 9.95 cm/k.y. occurs in the interval from the LO of *G. dehiscens* and the FO of *G. conglobatus* (6.2 Ma). Sedimentation rate increased to 11.8 cm/k.y. from the FO of *G. conglobatus* to the FO of *G. margaritae* (6.4 Ma). Between the FO of *G. margaritae* and the FO of *C. nitida* (8.1 Ma), the rate of sedimentation drastically decreased to 2.8 cm/k.y., whereas it increased again up to 6.85 cm/k.y. between the FO of *C. nitida* and the FO of *G. plesiotumida* (8.3 Ma). The next observed datum is the FO of *N. humerosa* (8.5 Ma), representing an interval of 200 k.y. with a sedimentation rate of ~19.25 cm/k.y. Sedimentation rate drastically decreased to 1.32 cm/k.y. between the FO of *N. humerosa* and the LO of the *P. siakensis/P. mayeri* group (11.4 Ma). An increase in the rate of sedimentation up to 8.9 cm/k.y. is observed between the LO of the *P. siakensis/P. mayeri* and the FO of *Z. nepenthes* (11.8 Ma). A further increase occurs in the interval between the FO of *Z. nepenthes* and the FO of *F. fohsi robusta*. This value, however, may not be real because of the very poor recovery of Core 166-1006A-71X. Finally, sedimentation rate decreased to 2.9 cm/k.y. between the FO of *F. fohsi robusta* (12.1 Ma) and the FO of *F. fohsi lobata* (12.5 Ma).

EARLY PLIOCENE–MIDDLE MIOCENE CYCLOSTRATIGRAPHY

In recent years, Neogene cyclic sedimentary successions have been shown to be paced by insolation variations caused by regular

Table 3. Position of main nannofossil biostratigraphic events.

Event	Age (Ma)	Horizon (sample between)	Depth (mbsf)
		166-1006A-	
T *Amaurolithus* spp.	4.5	28H-3, 114-115 cm/28H-5, 14-15 cm	259.24
B *Ceratolithus rugosus*	4.7	36X-1, 114-115 cm/36X-2, 14-15 cm	322.89
T *Discoaster quinqueramus*	5.6	38X-4, 14-15 cm/38X-4, 64-65 cm	344.69
B *Amaurolithus amplificus*	6.6	45X-1, 14-15 cm/45X-1, 64-65 cm	404.39
B *Amaurolithus primus*	7.2	46X-2, 14-15 cm/46X-3, 14-15 cm	415.79
B *Discoaster berggrenii*	8.6	54X- CC/55X-1, 14-15 cm	496.37
T *Discoaster hamatus*	9.4	59X-3, 14-15 cm/59X-CC	538.05
B *D. hamatus*	10.7	62X-6, 14-15 cm/62X-CC	571.83
B *Catinaster coalitus*	11.3	66X-2, 14-15 cm/66X-CC	603.83
T *Cyclicargolithus floridanus*	13.2	75X-CC/76X-1, 12-13 cm	695.56

Note: T = top, B = base. Depths measured at top of interval.

Table 4. Shipboard data on planktonic foraminiferal distribution at Site 1006, used in Figure 6.

Event	Zone	Age (Ma)*	Age (Ma)†	Depth (mbsf)
T *Globigerinoides obliquus*		1.3	1.3	69.35
T *Globigerinoides extremus*		1.77	1.98	88.2
B *Globorotalia truncatulinoides*	(N21/22)	2	1.92	97.69
T *Globorotalia exilis*		2.2	2.09	107.18
T *Globorotalia miocenica*		2.3	2.38	116.8
T *Globorotalia limbata*		2.4	2.38	135.36
T *Dentoglobigerina altispira*		3.09	3.11	145.42
B *Globorotalia tosaensis*	(N20/21)	3.2		154.78
B *G. miocenica*	(N19/20)	3.55	3.77	173.25
T *Globorotalia margaritae*		3.58	3.85	173.25
T *Zeaglobigerina nepenthes*		4.18	4.39	240.28
T *Globorotalia cibaoensis*		4.6		352.68
B *Sphaeroidinella dehiscens*	(N17/18)	5.2	5.54	383.42
B *Globigerinoides conglobatus*		6.2	6.2	436.04‡
B *G. margaritae*		6.4	6.09	454.96‡
B *G. cibaoensis*		7.7	9.44	483.07
B *G. extremus*		8.1	8.58	492.05
B *Neogloboquadrina acostaensis*	(N15/16)	10.9	9.82	595.39
T *Globotoralia mayeri*	(N14/15)	11.4	10.49	595.39
B *G. nepenthes*	(N13/14)	11.8	11.19	625.08
T *Fohsella* sp.	(N12/13)	11.9	11.68	639.96
B *F. fohsi*	(N11/12)	12.7	13.42	682.02

Note: T = top, B = bottom. * = after Berggren et al. (1995); † = after ODP Leg 154 (Curry, Shackleton, Richter, et al., 1995). ‡ = depths not used in Figure 6.
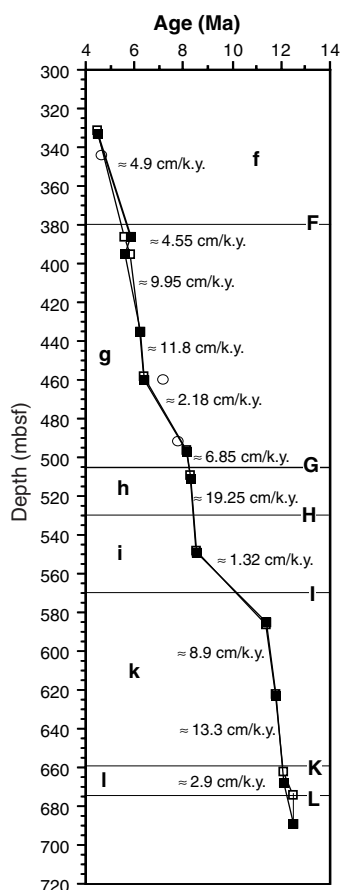

Figure 3. Age-depth plot of Hole 1006A based on the position of selected planktonic foraminiferal events (black squares). Open circles = position of planktonic foraminiferal events that have not been well calibrated yet and are, therefore, not used in the age-depth plot; open squares = uncertainty in the depth of the planktonic foraminiferal events; f through l = seismic sequences; F through L = position of seismic sequence boundaries after conversion into depth.

changes in the Earth's orbit and the orientation of the Earth's axis, and have been dated by correlation of the sediment cycles to the calculated insolation variations (Hilgen et al., 1991, 1995; Shackleton et al., 1990). At Site 1006, the sediment alternates between a light yellowish or greenish grey nannofossil ooze (neritic, high sea level) and a light grey (white) nannofossil ooze with foraminifers (pelagic, low sea level). In lithologic Units 3–5, the pelagic part is sometimes topped with a firmground or hardground and in Unit 1, the cycles often start with a basal clay layer (Eberli, Swart, Malone, et al., 1997).

These cycles are observed in most of the downhole logs. Compaction, cementation, and quantity of microfossils all affect porosity, which governs the neutron porosity, density, resistivity, and sonic velocity logs. The balance between carbonate and clays is reflected in the photoelectric factor (PEF) log. Calcite has a PEF of ~5 barn/e⁻, and clays typically have PEFs of 1.5–3.5 barn/e⁻. In addition, diamagnetic calcite has a negative magnetic susceptibility, whereas paramagnetic clays have a positive susceptibility. Color reflectance at 700 nm correlates with aragonite content (Eberli, Swart, Malone, et al., 1997). The (spectral) natural gamma-ray log has uranium as its principal source; uranium tends to accumulate at redox boundaries, and mark events such as hardgrounds (Serra, 1984; Williams and Pirmez, 1999), and, therefore, does not show ideal cyclic behavior. Potassium and thorium peaks mark occurrences of clay-rich sediment.

The character of the cycles changes at the boundary between Unit 2 and Unit 3, so the succession is treated in two parts: 180–360 mbsf (Fig. 4) and 360–715 mbsf (Fig. 5). The upper part of the hole (Pleistocene–late Pliocene) is not dealt with here.

In Unit 2 (126–360 mbsf), the resistivity (SFLU) log contains regularly spaced cycles recurring about every 1.4 m (Fig. 4). The same cycles are observed in the sonic velocity log, but are less clearly seen in the density and neutron porosity logs and FMS resistivity images (see figures in Eberli, Swart, Malone, et al., 1997) because the wide borehole in Unit 2 causes degraded contact between tool and borehole wall, which these logs require. Assuming a precessional periodicity of 22 k.y. per cycle, the sedimentation rate is ~6 cm/k.y.: about half that suggested by the biostratigraphy. Cycles in magnetic susceptibility measured on core appear to have a longer wavelength, giving a sedimentation rate of ~12 cm/k.y., in agreement with the biostratigraphy (Fig. 6; Tables 4, 5, 6, 7). It is likely that susceptibility is tracking the balance between clay and carbonate downhole. It appears that the distinct cycles in resistivity occur twice per precessional cycle. Resistivity is higher where there is more cementation, typically in the neritic-rich sediment. An initial interpretation of the behavior of the resistivity log is that the carbonate bank is exporting neritic-rich sediment twice per precessionally driven sea-level cycle, maybe indicating both highstand and lowstand shedding. The susceptibility traces variations in clay content, which depends on erosion in the source area (Cuba and Hispaniola), and current strength; magnetic susceptibility is largely independent of the sediment supply from the carbonate platform. It seems unlikely that the biostratigraphic picks over this interval should be far wrong, and their ages are well known, since they are astronomically dated in the Pliocene (Berggren et al., 1995a).

In Units 3–5 (360–715 mbsf), cycles in the resistivity, FMS image, and porosity logs were counted (Fig. 4). Each gave slightly different numbers of cycles, but this can be mostly attributed to the different vertical resolutions of the logs (SFLU resistivity ~45 cm, porosity ~30 cm, FMS image ~0.5cm). The resistive beds in the FMS image are mostly thin relative to the intervening less-resistive sediment, suggesting that they mark a distinct (though as yet unidentified) stage in the carbonate bank's cycle. The logged cycles are paced by precessional forcing, giving sedimentation rates comparable with those derived from the biostratigraphy (Fig. 6).

The reliability of the cycle stratigraphic depth-age line for Site 1006 has four main constraints, the latter three resulting from the first one. First, it is difficult to identify long-term eccentricity-controlled
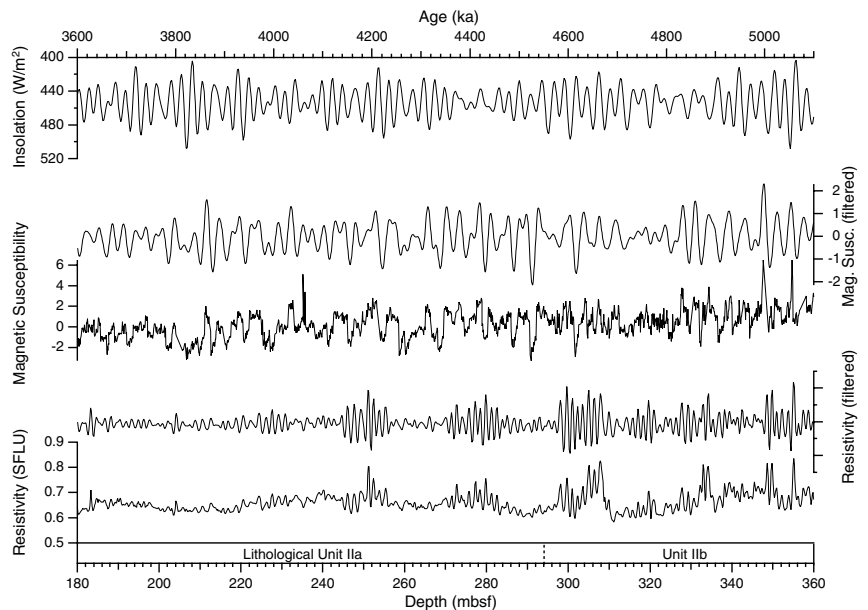
Figure 4. Cyclic variations in resistivity and magnetic susceptibility in lithologic Unit 2. Both have been band-pass filtered to bring out the cyclic component, and the summer insolation (65° N) curve (Paillard et al., 1996) for the interval is shown for comparison.

amplitude variations in the precessionally controlled log cycles at Site 1006. From the point of view of dating, this is a major problem because amplitude variation is the key to matching a specific sedimentary cycle to the corresponding insolation cycle (Hilgen et al., 1991, 1995; Shackleton et al., 1990). The porosity-related log cycles at Site 1006 are depositional features, but they are also diagenetically enhanced. During both of these processes, some of the proportionality to the original insolation/sea-level forcing may have been lost. Second, the cyclostratigraphy is 'floating,' and needs to be tied to a particular reliable biostratigraphic date. Third, a duration of 22 k.y. for each cycle was chosen (somewhat arbitrarily) to reflect the relative importance of the 23 k.y. over the 19-k.y. precessional periodicities. Fourth, the picking of cycles is subjective: whether a particular log peak represents a precessionally controlled cycle is not always clear. In an attempt to combat this, cycles were picked from several different logs.

A further difficulty in comparing the cyclostratigraphy to the biostratigraphy is that, in the Miocene, the Berggren et al. (1995b) ages for biostratigraphic dates are not astronomically calibrated. Thus, in Figure 6B, we show the Site 1006 biostratigraphic data with ages that were astronomically calibrated on ODP Leg 154 material from the Ceara Rise (Backman and Raffi, 1997; Chaisson and Pearson, 1997). The ODP Leg 154 tuned ages applied to the Site 1006 bioevents agree well with the predicted ages by the cyclostratigraphy, particularly in the interval 10–12 Ma. However, some astronomically calibrated bioevents (Figure 6B) ~13 Ma deviate more from the predicted sedimentation rate line than the ages of the bioevents as defined in Berggren et al. (1995b). There could be several reasons for this. Use of different taxonomic concepts by individual workers is always a potential for pitfalls. Also, diachroneity of planktonic foraminiferal bioevents is a factor that is not well understood. Therefore, it is impossible to know what has caused the differences and, as a consequence, it is not possible to calibrate the bioevents of Site 1006 because we have used a 'floating' cyclostratigraphy rather than a tuned stratigraphy. The absence of a strong paleomagnetic signal is hampering progress toward a tuned Milankovitch stratigraphy. At present, the cyclostratigraphic record is anchored on one bioevent. Progress could be made by using quantitative micropaleontology in the future to find a range of reliable bioevents to evaluate the position of the cyclostratigraphy with respect to the solar insolation curve (Backmann and Raffi, 1998). Nonetheless, the present cyclostratigraphy is extremely useful for evaluating Milankovitch-induced variations in sedimentation rate.

DISCUSSION AND CONCLUSIONS

The sedimentary sequence at Hole 1006A is remarkably continuous, expanded, and precisely dated. Therefore, this site is an excellent location to compare isotopic and sedimentary records and will probably become a classic site for late Cenozoic paleoceanography in the low-latitude Atlantic (Eberli, Swart, Malone, et al., 1997). The early Pliocene–middle Miocene bio-cyclostratigraphy shows that the sequence is complete and it provides an accurate estimate of sedimentation rates. The variation in sedimentation rates is crucial for understanding sediment production on the platform over time in relation to sea-level changes. Here, we have an ideal opportunity to study the Great Bahama Bank platform production from early Pliocene to middle Miocene times.

The variation of sedimentation rates in periplatform deposits is mainly controlled by the switching on and off of the carbonate factory during sea-level highstands and lowstands, respectively (Droxler and Schlager, 1985; Reijmer et al., 1988). During flooding, the platform produces increased amounts of neritic material that gets swept onto the upper slope of the basin (highstand shedding). In contrast, during lowstands, the platform production is drastically reduced and in some cases, during large sea-level falls, the platform might have been exposed. If exposed, coarser grained material is deposited onto the very upper slope (Rendle et al., Chap. 6, this volume). The Pleistocene sea-level cycles had a large effect on platform production and shedding of material toward the leeward side of the Great Bahama Bank (Kroon et al., Chap. 2, this volume; Rendle et al., Chap. 6, this volume) according to the above-described scenario. Here, we assume that a similar mechanism was responsible for the cyclic sedimentation in the lower Pliocene–middle Miocene record, although sea-surface temperature variations may also be important. At this stage, we can not prove exactly what caused the cyclic variations because paleoceanographic proxies such as stable oxygen isotope variations have not been produced as yet, but are in progress (McKenzie et el., 1998; McKenzie et al., unpubl. data). Also, the bank had more ramp-like morphology in the Miocene period, so it would have had a slightly different style of carbonate production over the sea-level cycle.

The cyclostratigraphy appears to be extremely useful for building an accurate 'floating' age model based on the assumption that precessional cycling forced the record. This assumption is reasonable because long-term sedimentation rate changes based on cyclostratigraphy are compatible with those based on biostratigraphy. By counting
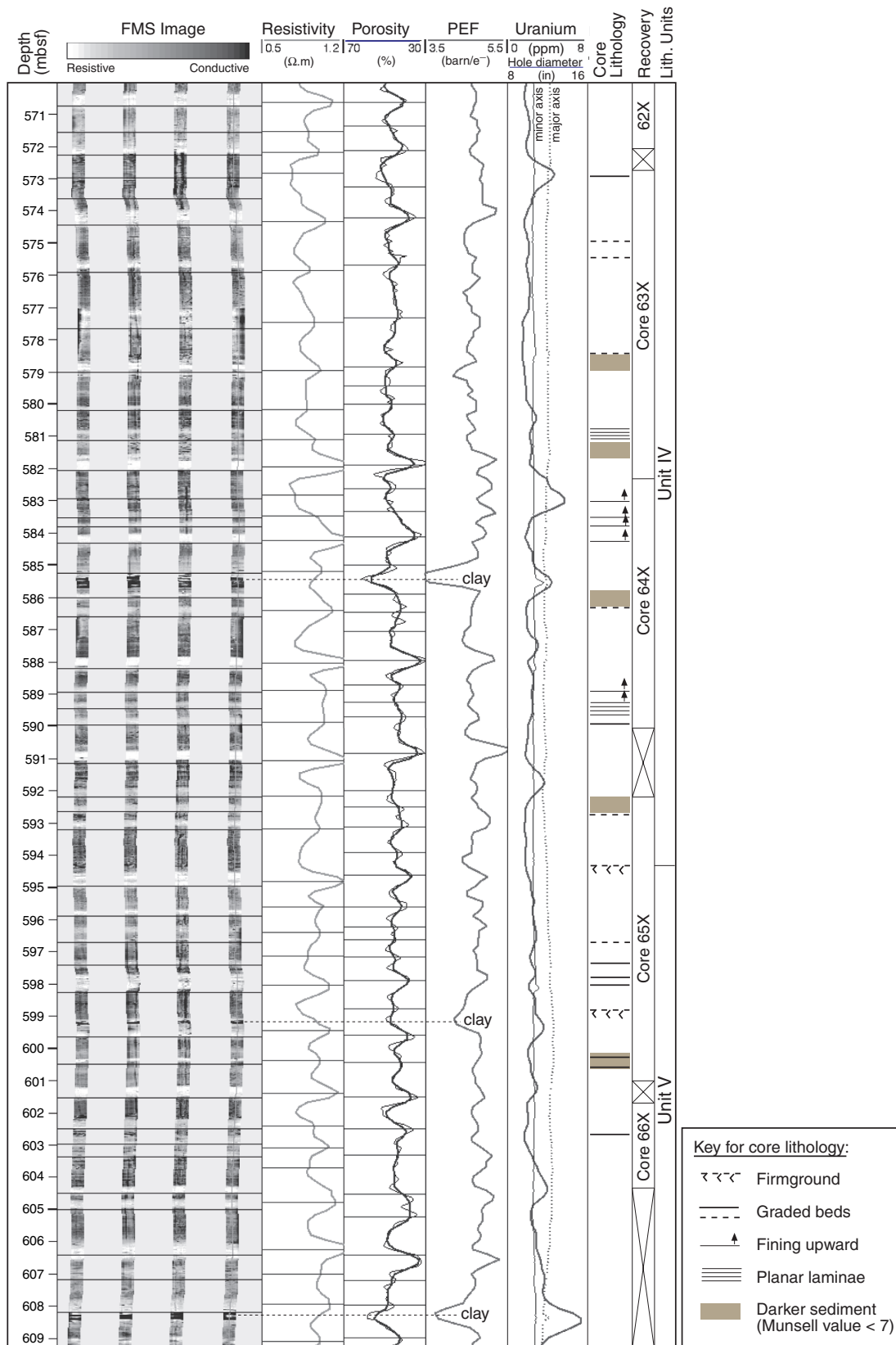
Figure 5. Cyclic variations in Formation MicroScanner (FMS) image resistivity, log resistivity (SFLU), porosity (APLC), photoelectric factor (PEF), uranium (HURA), and borehole diameter. Picked cycles are indicated by horizontal lines. Note also the occurrence of uncemented clay layers at 585.5, 599, and 608 mbsf.
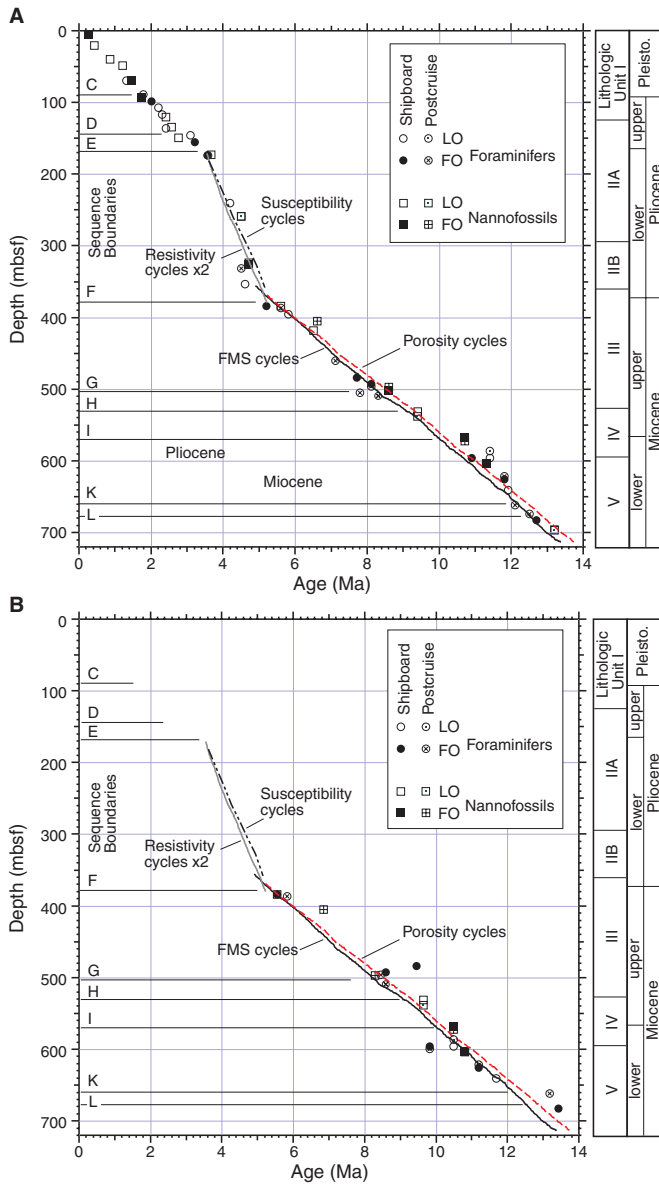
Figure 6. Depth-age plot showing foraminifer and nannofossil data and cycle stratigraphies using (**A**) Berggren et al. (1995) ages and (**B**) ODP Leg 154 ages for the bioevents. The bioevents used are given in Tables 4–7. C–L = sequence boundaries, LO = last occurrence, FO = first occurrence, FMS = Formation MicroScanner. The solid and dashed line represent the predicted age-depth plot by using the cyclostratigraphy of the FMS and porosity cycles. The bioevents at Site 1006 reasonably close to the predicted line by applying the Berggren et al. (1995) ages (A), although clear deviations can be seen at ~10–12 Ma. The bioevents at ~10–12 Ma fit much better when the tuned ODP Leg 154 ages are applied, although two events ~13.2 Ma are offset from the line. This is probably caused by problems with taxonomic interpretations.

the cycles induced by precessional forcing, accurate sedimentation rate variations can be calculated.

The sedimentation rate at Site 1006 generally varies between 4 and 8 cm/k.y. (Fig. 7), apart from the faster rates of ~5–20 cm/k.y. in Unit 2 (3.6–4.6 Ma). The higher rates are above normal rates of pelagic sedimentation, particularly at the extreme upper end of its range. Carbonate fluxes (there is not much terrigenous material in this section) must have been very high to increase sedimentation rates

Table 5. Postcruise data on planktonic foraminiferal distribution at Site 1006 used in Figure 6.

Event	Age (Ma)*	Age (Ma)†	Depth (mbsf)
B *Globotoralia crassaformis*	4.5		331.45
T *Globorotalia cibaoensis*	4.6		
B *Globorotalia aemiliana*			358.95
B *Neogloboquadrina pseudopima*			364.95
B *Globorotalia tumida*	5.6	5.82	385.95
T *Globoquadrina dehiscens*	5.8		395.05
T *Globorotalia lenguaensis*	6		395.05‡
B *Globigerinoides conglobatus*	6.2	6.2	434.85‡
B *Globorotalia margaritae*	6.4		458.45‡
B *Globorotalia conomiozea*	7.12		460.15
B *G. cibaoensis*	7.8		491.05‡
B *Candeina nitida*	8.1	8.44	495.55
B *Globorotalia juanai*	8.1		500.15‡
T *Polipheribola christiani*			501.66
B *Globorotalia suterae*	7.8		504.65
B *Globorotalia mediterranea*			506.25
B *Globorotalia plesiotumida*	8.3	8.58	509.25
B *Globigerinoides extremus*	8.3	8.58	509.25
B *Globorotalia sphericomiozea*			509.25
B *Globorotalia merotumida*			517.35
B *Neogloboquadrina humerosa*	8.5		547.75‡
B *P. christiani*			549.25
T *Paragloborotalia siakensis/P. mayeri*	11.4	10.49	586.25
B *Neogloboquadrina acostaensis*		9.82	598.95
B *Globorotalia menardii*			618.25
B *Zeaglobigerina nepenthes*	11.8	11.19	621.25
B *Globorotalia praemenardii*			631.35
B *Fohsella fohsi robusta*	12.1	13.18	661.72
B *Fohsella fohsi lobata*	12.5		673.57

Note: T = top, B = bottom.* = after Berggren et al. (1995); † = after ODP Leg 154 (Curry, Shackleton, Richter, et al., 1995). ‡ = depths not used in Figure 6.

Table 6. Shipboard nannofossil distribution data from Site 1006 used in Figure 6.

Event	Zones	Age (Ma)*	Age (Ma)†	Depth (mbsf)
B *Emiliania huxleyi*	(NN20/21)	0.25		4.24
T *Pseudoemiliania lacunosa*	(NN19/20)	0.41		20.53
T *Reticulofenestra asanoi*		0.85		39.53
T *Gephyrocapsa* spp. (large)		1.2		48.49
B *Gephyrocapsa* spp. (large)		1.44		68.03
B *Gephyrocapsa caribbeanica*	(NN18/19)	1.72		91.78
T *Discoaster pentaradiatus*		2.4		120.28
T *Discoaster surculus*		2.56		134.33
T *Discoaster tamalis*		2.75		148.78
T *Reticulofenestra pseudoumbilicus*	(NN15/16)	3.66		172.53
T *Amaurolithus* spp.		4.5		258.62
B *Ceratolithus rugosus*		4.7		325.98
T *Discoaster quinqueramus*	(NN11/12)	5.6	5.537	383.42
T *Reticulofenestra* (small)		6.5		417.8
B *D. quinqueramus*	(NN10/11)	8.6		500.95
T *Discoaster hamatus*	(NN9/10)	9.4	9.635	530.48
B *D. hamatus*	(NN8/9)	10.7	10.476	567.45
B *Catinaster coalitus*	(NN7/8)	11.3	10.794	602.51
T *Cyclicargolithus floridanus*	(NN6/7)	13.2		696.27

Note: T = top, B = bottom.* = after Berggren et al. (1995); † = after ODP Leg 154 (Curry, Shackleton, Richter, et al., 1995).

Table 7. Postcruise data on nannofossil distribution at Site 1006 used in Figure 6.

Event	Age (Ma)*	Age (Ma)†	Depth (mbsf)
T *Amaurolithus* spp.	4.5		259.24
B *Ceratolithus rugosus*	4.7		322.89
T *Discoaster quinqueramus*	5.6	5.537	344.69‡
B *Amaurolithus amplificus*	6.6	6.84	404.39
B *Amaurolithus primus*	7.2		415.79‡
B *Discoaster berggrenii*	8.6	8.281	496.37
T *Discoaster hamatus*	9.4	9.635	538.05
B *D. hamatus*	10.7	10.476	571.83
B *Catinaster coalitus*	11.3	10.794	603.83
T *Cyclicargolithus floridanus*	13.2		695.56

Note: T = top, B = bottom. * = after Berggren et al. (1995); † = after ODP Leg 154 (Curry, Shackleton, Richter, et al., 1995). ‡ = depths not used in Figure 6.

above normal pelagic and thus the carbonate platform was also shedding material to the slope throughout the cored interval.

The faster sedimentation rate of ~5–20 cm/k.y. (Fig. 7) in Unit 2 (3.6–4.6 Ma) coincides with the interval where there are two resistivity log peaks per precessional cycle, and also where there is an absence of hardgrounds. It is not known why the resistivity log shows a double peak. The precessional cycle is evident in the cores by alternating dark and grey layers. Light grey wackestones/packstones contain high amounts of fine-grained shallow-water bioclasts. Dark grey wackestones/packstones are dominated by pelagic components and contain up to 15% clay (Betzler et al., unpubl. data). The lithology, therefore, suggests a highstand vs. a lowstand deposit during a sea-level cycle at the precessional frequency. However, there is not a clear lithological expression of a double cycle in the cores; thus, the resistivity signal must respond to different parameters that are not yet known such as cyclical cementation horizons.

The elevated sedimentation rates in Unit 2 (Fig. 8) started shortly after the Miocene/Pliocene boundary (5.33 Ma; Hilgen et al., 1995), which occurs at 371 mbsf according to the biostratigraphy. The cyclostratigraphy would put the boundary at similar levels, albeit slightly deeper in the section at 375 mbsf. The timing of the increase in sed-

imentation rate coincides with the final step in the closure of the Panama Isthmus. We suspect that the closure led to reorganization of surface currents in the Florida Strait and Santaren Channel and the location and strength of the currents may have contributed in shifting depositional centers in the Strait. Another possibility is increased platform shedding into the basin expanding the lower Pliocene section. However, not all the records of Leg 166 sites drilled higher up the slope show an expanded section in this time interval and thus the change in currents and depocenter location is the more likely scenario.

The sedimentation rate changes in Figure 8 show cyclicity at long wavelengths. Spectral analysis of this time-series (Fig. 9) reveals that most of the variability in sedimentation rate is at periodicities of 88, 124, 440, and 1800 k.y., which are very similar to known periodicities in the orbital eccentricity (96, 125, 400, and 2000 k.y.). The pulses of sediment from the bank are paced by the precessional cycle. Thus, the platform produced a carbonate pulse every precessional cycle, through its control on sea level, and perhaps also its control on temperature as a direct result of low-latitude insolation. From our analysis of the sedimentation rate record, the amount of carbonate material shed into the basin during those pulses is controlled by ec-
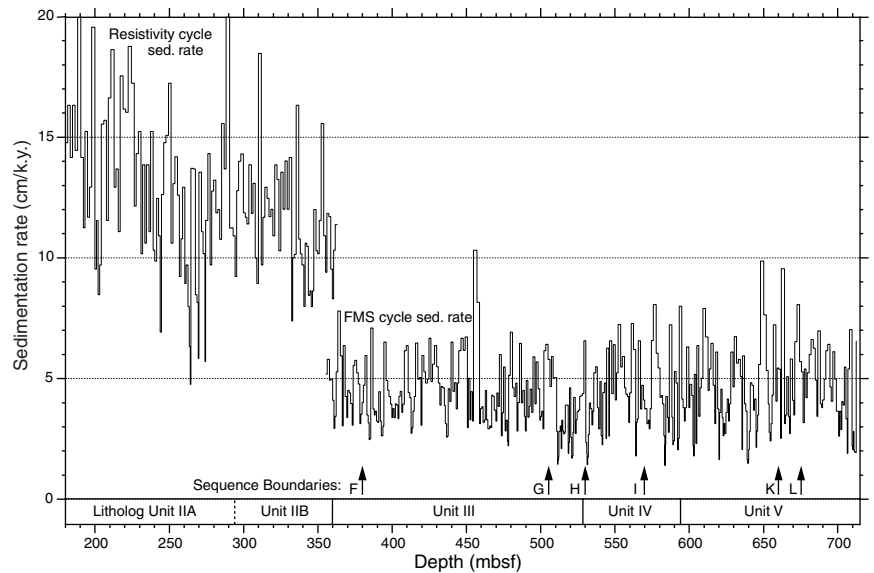

Figure 7. Sedimentation rate variability vs. depth. FMS = Formation MicroScanner, F through L = sequence boundaries from Eberli et al.(1997).
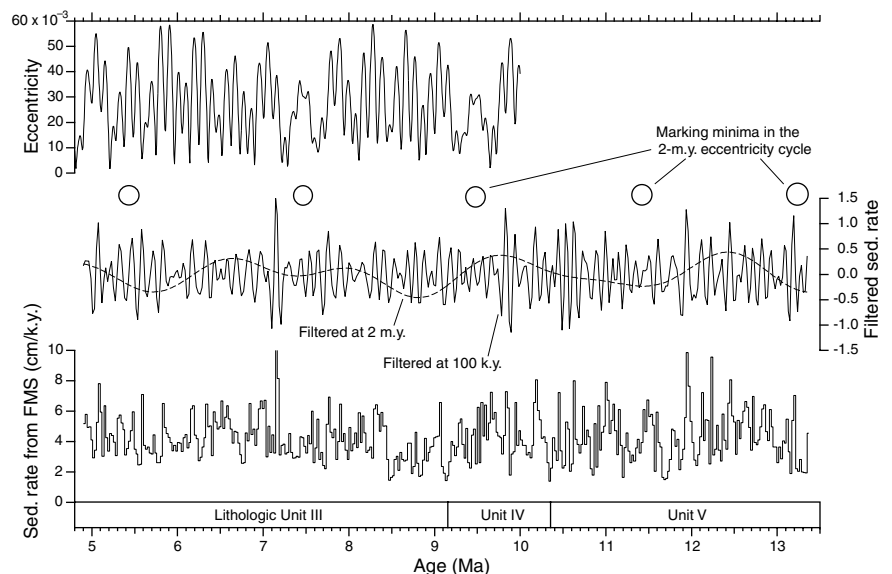

Figure 8. Sedimentation rate variability vs. time. FMS = Formation MicroScanner. The filtered sedimentation rate record shows the occurrences of the short- and long-term eccentricity cycles. Also, the long-term 1.8-m.y. cycle is indicated by the dashed line. The maxima in sedimentation rates are interpreted as periods of high-carbonate platform input onto the upper slope as a consequence of sea-level highstands. The sedimentation rate fluctuations could therefore be interpreted as a sea-level curve throughout the middle-upper Miocene. The observation that the short- and long-term eccentricity cycles are pervasive throughout the record is important.
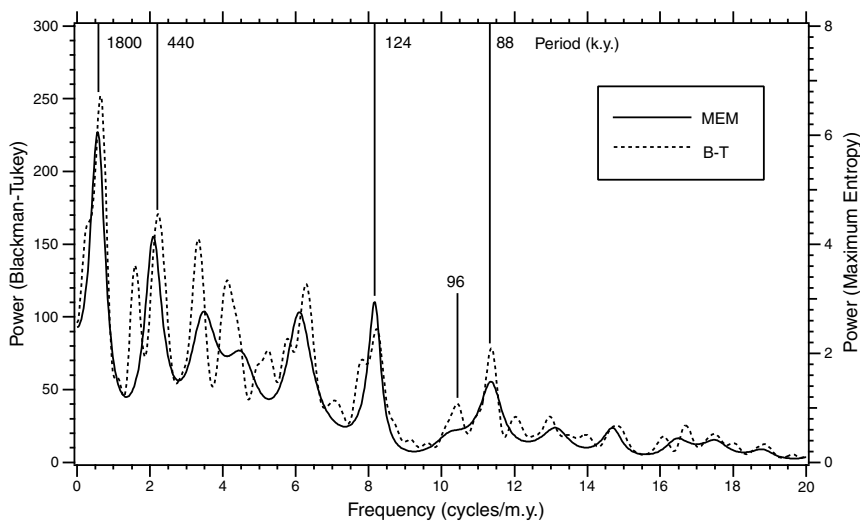
Figure 9. Maximum Entropy (MEM) and Blackman-Tukey (B–T) spectral analysis of the sedimentation rate as shown in Figure 8. The resulting periodicities are close to the known periodicities in orbital eccentricity (96, 125, 440, and 2000 k.y.).

centricity, likely because eccentricity modulates the amplitude of the precessional insolation cycle and, therefore, the amplitude of the sea-level variation. It appears that when the platform experiences a sea-level cycle of higher amplitude, it produces and exports more carbonate than when the sea-level cycle is more modest. Short- and long-term eccentricity modulation of the precessional cycles resulted in periods of extreme and minimal platform production.

We conclude that the logs reveal the sedimentation rate variations at Site 1006. The sedimentation rate changes are interpreted to be controlled by both platform production and variability of the currents. The sedimentation rate variations occur in regular cycles controlled by orbital eccentricity. The bundling of precessional cycles into packets of 100 k.y., 400 k.y., and 2 m.y. shows that eccentricity plays an important role in modulating the amplitude of sea-level changes during a period when there was less ice than in the Pleistocene.

ACKNOWLEDGEMENTS

REFERENCES

Backman, J., and Raffi, I., 1997. Calibration of Miocene nannofossil events to orbitally tuned cyclostratigraphies from Ceara Rise. *In* Shackleton, N.J., Curry, W.B., Richter, C., and Bralower, T.J. (Eds.), *Proc. ODP, Sci. Results,* 154: College Station, TX (Ocean Drilling Program), 83–99.

Barbieri, R., 1998. Foraminiferal paleoecology at the Tortonian-Messinian boundary, Atlantic coast of Northwestern Morocco. *J. Foraminiferal. Res.,* 28:102–123.

Berggren, W.A., 1973. The Pliocene time scale: calibration of planktonic foraminiferal and calcareous nannoplankton zones. *Nature,* 243:391–397.

Berggren, W.A., Hilgen, F.J., Langereis, C.G., Kent, D.V., Obradovich, J.D., Raffi, I., Raymo, M.E., and Shackleton, N.J., 1995a. Late Neogene chronology: new perspectives in high-resolution stratigraphy. *Geol. Soc. Am. Bull.,* 107:1272–1287.

Berggren, W.A., Kent, D.V., Swisher, C.C., III, and Aubry, M.-P., 1995b. A revised Cenozoic geochronology and chronostratigraphy. *In* Berggren, W.A., Kent, D.V., Aubry, M.-P., and Hardenbol, J. (Eds.), *Geochronology, Time Scales and Global Stratigraphic Correlation.* Spec. Publ.— Soc. Econ. Paleontol. Mineral. (Soc. Sediment. Geol.), 54:129–212.

Bermúdez, P.J., 1949. Tertiary smaller foraminifera of the Dominican Republic. *Spec. Publ.Cushman Lab. Foraminiferal Res.,* 25.

Blow, W.H., 1969. Late middle Eocene to Recent planktonic foraminiferal biostratigraphy. *In* Brönnimann, P., and Renz, H.H. (Eds.), *Proc. First Int. Conf. Planktonic Microfossils, Geneva, 1967:* Leiden (E.J. Brill), 1:199–422.

————, 1979. The Cainozoic Globigerinida: Leiden (E.J. Brill).

Bolli, H.M., and Saunders, J.B., 1985. Oligocene to Holocene low latitude planktic foraminifera. *In* Bolli, H.M., Saunders, J.B., and Perch-Nielsen, K. (Eds.), *Plankton Stratigraphy:* Cambridge (Cambridge Univ. Press), 155–262.

Brönnimann, P., and Resig, J., 1971. A Neogene globigerinacean biochronologic time-scale of the Southwestern Pacific. *In* Winterer, E.L., Riedel, W.R., et al., *Init. Repts. DSDP,* 7 (Pt. 2): Washington (U.S. Govt. Printing Office), 1235–1469.

Chaisson, W.P., and Pearson, P.N., 1997. Planktonic foraminifer biostratigraphy at Site 925: middle Miocene–Pleistocene. *In* Shackleton, N.J., Curry, W.B., Richter, C., and Bralower, T.J. (Eds.), *Proc. ODP, Sci. Results,* 154: College Station, TX (Ocean Drilling Program), 3–31.

Cita, M.B., 1975. Studi sul Pliocene e gli strati di passaggio dal Miocene al Pliocene, VII. Planktonic foraminiferal biozonation of the Mediterranean Pliocene deep sea record: a revision. *Riv. Ital. Paleontol. Stratigr.,* 81:527–544.

Cita, M.B., and Gartner, S., 1973. Studi sul Pliocene e sugli strati al passaggio dal Miocene al Pliocene. IV. The stratotype Zanclean foraminiferal and nannofossil biostratigraphy. *Riv. Ital. Paleontol. Stratigr.,* 79:503–558.

Colalongo, M.L., and Sartoni, S., 1967. *Globorotalia hirsuta aemiliana* nuova sottospecie cronologica del Pliocene in Italia. *G. Geol.,* 34:1–15.

Curry, W.B., Shackleton, N.J., Richter, C., et al., 1995. *Proc. ODP, Init. Repts.,* 154: College Station, TX (Ocean Drilling Program).

Droxler, A.W., and Schlager, W., 1985. Glacial versus interglacial sedimentation rates and turbidite frequency in the Bahamas. *Geology,* 13:799–802.

Eberli, G.P., Swart, P.K., Malone, M.J., et al., 1997. *Proc. ODP, Init. Repts.,* 166: College Station, TX (Ocean Drilling Program).

Fleisher, R.L., 1974. Cenozoic planktonic foraminifera and biostratigraphy, Arabian Sea, Deep Sea Drilling Project, Leg 23A. *In* Whitmarsh, R.B., Weser, O.E., Ross, D.A., et al., *Init. Repts. DSDP,* 23: Washington (U.S. Govt. Printing Office), 1001–1072.

Foresi, L.M., Iaccarino, S., Mazzei, R., and Salvatorini, F., 1998. New data on middle to late Miocene calcareous plankton biostratigraphy in the Mediterranean area. *Riv. Ital. Paleontol. Stratigr.,* 104:95–114.

Hilgen, F.J., 1991. Extension of the astronomically calibrated (polarity) time scale to the Miocene/Pliocene boundary. *Earth Planet. Sci. Lett.,* 107:349–368.

Hilgen, F.J., Krijgsman, W., Langereis, C.G., Lourens, L.J., Santarelli, A., and Zachariasse, W.J., 1995. Extending the astronomical (polarity) time scale into the Miocene. *Earth Planet. Sci. Lett.,* 136:495–510.

Hsü, K.J., Montadert, L., et al., 1978. *Init. Repts. DSDP,* 42 (Pt. 1): Washington (U.S. Govt. Printing Office).

Kennett, J.P., and Srinivasan, M.S., 1983. *Neogene Planktonic Foraminifera: A Phylogenetic Atlas:* Stroudsburg, PA (Hutchinson Ross).

Martini, E., 1971. Standard Tertiary and Quaternary calcareous nannoplankton zonation. *In* Farinacci, A. (Ed.), *Proc. 2nd Int. Conf. Planktonic Microfossils Roma:* Rome (Ed. Tecnosci.), 2:739–785.

McKenzie, J.A., Spezzaferri, S., Anselmetti, F., and Isern, A., 1998. Linking isotope records eustasy to sequence stratigraphic patterns along the Baha-

mas sea-level transect: results from ODP Leg 166, Site 1006A. *ICP VI, Lisbon,* 163.

McKenzie, J.A., Spezzaferri, S, and Isern, A., in press. The Miocene/ Pliocene boundary in the Mediterranean and Bahamas: implications for a global flooding event in the earliest Pliocene. *Mem. Soc. Geol. Ital. Spec. Publ.*

McKenzie, J.A., Sprovieri, R., and Channell, J.E.T., 1990. The terminal Messinian flood and earliest Pliocene paleoceanography in the Mediterranean: results from ODP Leg 107, Site 652, Tyrrhenian Sea. *Mem. Soc. Geol. Ital.,* 44:81–91.

Müller, C., and Spiegler, D., 1993. Revision of late/middle Miocene boundary on the Voering Plateau (ODP Leg 104). *Newsl. Stratigr.,* 28:171–178.

Paillard, D., Labeyrie, L., and. Yiou, P., 1996. Macintosh program performs time-series analysis. *Eos,* 77:379.

Poore, R.Z., 1979. Oligocene through Quaternary planktonic foraminiferal biostratigraphy of the North Atlantic: DSDP Leg 49. *In* Luyendyk, B.P., Cann, J.R., et al., *Init. Repts. DSDP,* 49: Washington (U.S. Govt. Printing Office), 447–517.

Premoli Silva, I., Castradori, D., and Spezzaferri, S., 1993. Calcareous nannofossil and planktonic foraminifer biostratigraphy of Hole 810C (Shatsky Rise, northwestern Pacific). *In* Natland, J.H., Storms, M.A., et al., *Proc. ODP, Sci. Results,* 132: College Station, TX (Ocean Drilling Program), 15–36.

Reijmer, J.J.G., Schlager, W., and Droxler, A.W., 1988. ODP Site 632: Pliocene-Pleistocene sedimentation cycles in a Bahamian basin. *In* Austin, J.A., Jr., Schlager, W., et al., *Proc. ODP, Sci. Results,* 101: College Station, TX (Ocean Drilling Program), 213–220.

Ryan, W.B.F., Hsü, K.J., et al., 1973. *Init. Repts. DSDP,* 13 (Pts. 1 and 2): Washington (U.S. Govt. Printing Office).

Serra, O., 1984. *Fundamentals of Well-Log Interpretation* (Vol. 1): *The Acquisition of Logging Data:* Dev. Pet. Sci., 15A: Amsterdam (Elsevier).

Shackleton, N.J., Berger, A., and Peltier, W.A., 1990. An alternative astronomical calibration of the lower Pleistocene timescale based on ODP Site 677. *Trans. R. Soc. Edinburgh: Earth Sci.,* 81:251–261.

Spezzaferri, S., 1994. Planktonic foraminiferal biostratigraphy and taxonomy of the Oligocene and lower Miocene in the oceanic record: an overview. *Palaeontographica Ital.,* 81:1–187.

————, 1998. Planktonic foraminifer biostratigraphy and paleoenvironmental implications of Leg 152 sites (East Greenland Margin). In Saunders, A.D., Larsen, H.C., and Wise, S.W., Jr. (Eds.), Proc. ODP, Sci. Results, 152: College Station, TX (Ocean Drilling Program), 161–189.

Spezzaferri, S., Cita, M.B., and McKenzie, J.A., 1998. The Miocene/ Pliocene boundary in the Eastern Mediterranean: results from Sites 967 and 969. *In* Robertson, A.H.F., Emeis, K.-C., Richter, C., and Camerlenghi, A. (Eds.), *Proc. ODP, Sci, Results.* 160: College Station, TX (Ocean Drilling Program), 9–28.

Spiegler, D., and Müller, C., 1992. Correlation of *Bolboforma* zonation and nannoplankton stratigraphy in the Neogene of the North Atlantic: DSDP Sites 12-116, 49-408, 81-555 and 94-608. *Mar. Micropaleontol.,* 20:45–58.

Vincent, E., 1975. Neogene planktonic foraminifera from the Central North Pacific, Leg 32, Deep Sea Drilling Project. *In* Larson, R.L., Moberly, R., et al., *Init. Repts. DSDP,* 32: Washington (U.S. Govt. Printing Office), 765–801.

Williams, T., and Pirmez, C., 1999. FMS images from carbonates of the Bahama Bank Slope, ODP Leg 166: lithological identification and cyclostratigraphy. *In* Lovell, M.A., Williamson, G., and Harvey, P.K. (Eds.), *Borehole Imaging: Application and case histories.* Geol. Soc. Spec. Publ. London, 159:227–238.